Advances in Robotics & Automation
ISSN: 2168-9695

Du et al., Adv Robot Autom 2015, S2:1
DOI: 10.4172/2168-9695.1000s2-006

Research Article Open Access

Modeling and Control of a Dragonfly-like Micro Aerial Vehicle

Du CP[1,2]*, Xu JX[2] and Zheng Y[1]

[1]School of Aeronautics and Astronautics, Zhejiang University, Hangzhou, 310027, China
[2]Department of Electrical and Computer Engineering, National University of Singapore, 117576, Singapore

Abstract

The modeling and control design of a dragonfly-like flapping wing micro aerial vehicle (FWMAV) are studied in this paper. The aerodynamic force model of flapping wings is presented first, which is obtained by the local air velocity of the wing and local attack angle of the wing, unlike some existing works. Then, the complete mathematic model of FWMAV is developed by combining the aerodynamic force model and a kinematic model in which the micro aerial vehicle is regarded as a 6 degree-of-freedom rigid body. To mimic real dragonflies, the tail of the FWMAV swings only, unlike fixed-wing aircrafts that possess conventional control surfaces in tail. This yields a control difficulty due to the loss of the maneuverability in tail. To design an appropriate control mechanism, the complete FWMAV model, which is highly nonlinear, is rewritten in a companion form. The controller is designed to iteratively solve for a desired control signal profile by means of a dual-loop nonlinear dynamic inversion with Newton-Raphson solution. Numerical simulation results show that the effectiveness and convergence performance of the nonlinear controller are obtained.

Keywords: Dragonfly-like flapping wing micro-aerial-vehicle; Mathematical model; Non-linear dynamic inversion; Controller design

Introduction

The purpose of this research is to model and control a dragonfly-like flapping wing micro aerial vehicle (FWMAV). It is well known that micro aerial vehicle (MAV) designs can be classified as fixed wing, rotary wing and flapping wing. Fixed wing MAV is capable of fast forward flight, which is suitable for flying outdoor. Rotary wing MAV is suitable for movement at low speed. Recently, flapping wing MAV has drawn a great deal of attention owing to its biomimetic characteristics, for instance the high energy efficiency during flight, flexibility in maneuverability, agility at low speed, low actuation noise, etc., which yield various potential applications, specifically for flying in a complex environment, including indoor reconnaissance and surveillance, exploration in woods, or in dull-dirty-dangerous environments. The flight of flapping wing MAV, such as bird-like robot and insect-like robot, is more complex than flight with fixed or rotary wing, because the beating motion of flapping wings is the only means that can counter the gravity force and propel themselves against aerodynamic drag.

There are many flapping wing creatures in the natural world. The structure and function of biological systems evolved optimally through a long period have many superior characteristics which scientists and engineers still cannot fully discover and produce. Inspired by the unique characteristics of the insects or birds, researchers have placed a great emphasis on the development of insect-like or bird-like robots [1-5]. In many existing works it was recognized that dragonflies are one of the oldest flying species and are known to have particularly superior flight abilities among the flying insects on earth [6-12]. Dragonflies can control four natural wings and can make various flying patterns such as fast flight, hovering, quick turn, etc.

Jung et al. identify the linear and nonlinear dynamics of the Stanford DragonFly UAV using data taken from flight tests and propose a discrete sliding mode control scheme to control and stabilize the longitudinal dynamics [6]. However the Stanford dragonfly UAV is not a flapping wing MAV but a fixed wing MAV.

The dynamics of a dragonfly-like robot is studied [7]. Its performance is analyzed in terms of time response and robustness by computational simulation based on the mathematical model of dragonfly-like robot, and an integer PID and a fractional PID controller were applied. It is noted that the robot has only one pair of the flapping wings and a traditional control surface tail. Quoc-Viet et al. present an insect-like MAV with two fixed wings, two flapping wings and a conventional-control-surface tail [8]. These MAVs all have the conventional-control-surface tail, which can achieve the higher effect of longitudinal and latitudinal control than tailless MAV, but differ from real dragonflies.

The effect of moment changes in the tailless flapping wing platform is studied [9], in order to pave the way of utilizing the effect for flight control of tailless flapping wing MAV. It shows that the nonlinearities of the tailless flapping wing MAV could yield a huge challenge.

The primary challenge in controlling the dragonfly-like MAV is due to the lack of a complete system model, which becomes necessary when dealing with the inherent instability of the MAV system and the complex fluid–structure interactions [13]. In this work, the complete mathematic model of FWMAV is developed by combining the aerodynamic force model and a kinematic model in which the micro aerial vehicle is regarded as a 6 degree-of-freedom rigid body. Due to the limited deflection of the activities in head and tail, a nonlinear dynamic inverse controller is adopted with Newton-Raphson solution. Comparing with existing works, the main contributions of our work lie in three aspects.

(1) Instead of adopting two flapping wings or conventional control surfaces for the tail, we drive forces and torques with an active head, four flapping wings, and an active tail without conventional-control-surface, which is more like biological dragonflies.

***Corresponding author:** Du CP, School of Aeronautics and Astronautics, Zhejiang University, Hangzhou, 310027, China, Tel: +86 571 8517 2244; E-mail: duchangping@zju.edu.cn

Received September 18, 2015; **Accepted** October 13, 2015; **Published** October 23, 2015

Citation: Du CP, Xu JX, Zheng Y (2015) Modeling and Control of a Dragonfly-like Micro Aerial Vehicle. Adv Robot Autom S2: 006. doi: 10.4172/2168-9695.S2-006

(2) The aerodynamic force and moment are derived analytically, which are produced from the active head, active tail, wings, flapping frequency, and stroke angle of wings. Furthermore, the aerodynamic force is obtained by the local air velocity and local attack angle of the wing, unlike the aerodynamic force [7,11,12] which is not suitable for hovering due to using the freedom air velocity.

(3) The complete FWMAV model, which is highly nonlinear, is rewritten in a companion form. The controller is designed to iteratively solve for a desired control signal profile by means of a dual-loop nonlinear dynamic inversion with Newton-Raphson solution.

The outline of this paper is as follows. In Section 2, the aerodynamic force model is proposed, and we develop the mathematical model of dragonfly-like FWMAV based on the 6 degree-of-freedom kinematical model of the rigid body. Section 3 gives the controller design for the dragonfly-like FWMAV. Numerical examples are carried out to validate the effectiveness of the controller in Section 4. Section 5 concludes the paper with a brief summary.

Modeling of the Dragonfly-like FWMAV

In this section, the model of the dragonfly-like FWMAV is given to study its motion and control problem. In nature, the dragonfly obtains the aerodynamic force by flapping wings, which is opposite to the weight of the dragonfly. Although the wings do move relative to the dragonfly's body, their mass is within 1%~5% of total dragonfly's mass [2,10-11]. The inertia effect of dragonfly's wings on dynamic model is relatively small and can be neglected during flapping stroke. Thus we assume that the dragonfly's body motion evolves according to the rigid body motion equations subject to external forces acting on its center of mass.

Sketch map of dragonfly-like FWMAV

Figure 1 shows the top view of the dragonfly, which contains an active head, an active tail, a body and four flapping wings. Coordinate system $ox_by_bz_b$ is defined as the body coordinate system of the dragonfly as shown in Figure 1. For simplicity, we assume that the head and tail of the dragonfly can swing in the level and vertical to change the moments of the dragonfly.

The origin of the body coordinate system 'o' is fixed at the centre of the dragonfly's gravity. The x-axis of the body coordinate system ox_b is inside the symmetric plane of the dragonfly. The y-axis of the body coordinate system oy_b is perpendicular to symmetric plane of the dragonfly and is rightward. oz_b is the z-axis of the body coordinate system. M_x, M_y, M_z are the moments in the body coordinate system.

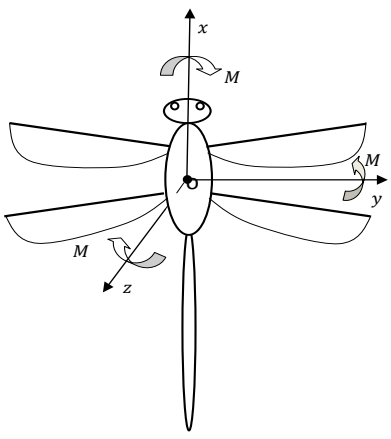

Figure 1: Sketch map of the dragonfly.

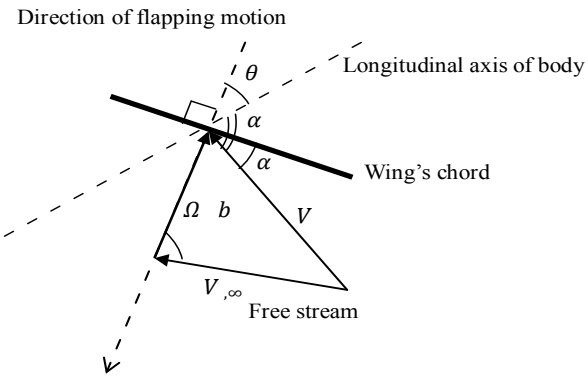

Figure 2: Lateral view of the dragonfly.

Remark 1: In our model, the active tail is modeled like a stick, which is more like a real dragonfly. On the contrast, in existing works the active tail is modeled as the conventional-control-surface, which is not realistic and generally used in fixed-wing UAV. It should be noted that conventional-control-surface provides much more powerful maneuverability with additional wings and control-surfaces. In comparison, the realistic stick-like tail is much difficult to control.

Aerodynamic force

When there is relative motion between the dragonfly's wings and the surrounding air, the aerodynamic force is yielded. In order to describe the force generation, some definitions are given below. The projection in the symmetric plane of local air velocity of the wings is shown in Figure 2.

$V_{\|}$ is the projection in the symmetric plane of local air velocity of the wings. $V_{\|,\infty}$ is the projection in the symmetric plane of freestream velocity. Ω is the flapping angular velocity. b is the equivalent span length. α_{bw} is the angle between the longitudinal axis of dragonfly's body and the local air velocity in the symmetric plane of the dragonfly. α_w is the angle between the wing's chord and the local air velocity in the symmetric plane of the dragonfly. θ_p denotes the angle from the x-axis of body coordinate system to flapping direction.

The origin of the wing coordinate system and the velocity coordinate system, o is defined at the centre of the dragonfly's gravity. The axis ox_w of the wing coordinate system is located inside the symmetric plane of the dragonfly, which is parallel to the wing's chord. The axis oy_w of the wing coordinate system is the same as the axis oy_b of the body coordinate system. The last axis oz_w of the wing coordinate system is determined by the right-hand screw rule. The axis ox_v of the velocity coordinate system is parallel to the air velocity. The axis oy_v and oz_v are y-axis, z-axis of the velocity coordinate system respectively.

Coordinate system $ox_zy_zw_z$ is defined as the wing coordinate system of the dragonfly as shown in Figure 3. The coordinate system $ox_vy_vw_v$ is defined as the velocity system of the dragonfly as shown in Figure 3. The ground coordinate system $ox_gy_gw_g$ is shown in Figure 4.

The origin of the ground coordinate system, o is fixed at a point on the ground. The axis ox_g and oy_g is located inside the horizontal plane,

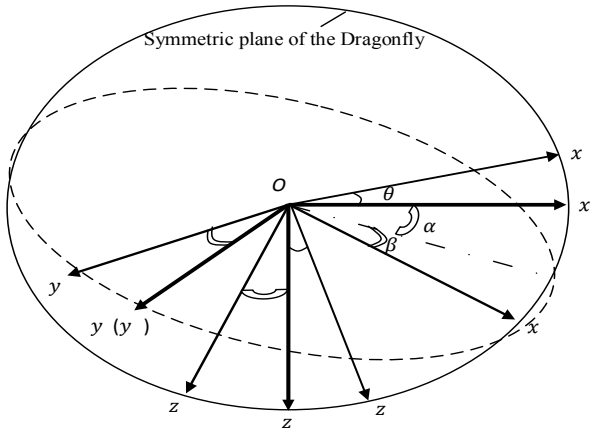

Figure 3: The relationship of the body coordinate system, the wing coordinate system and the velocity coordinate system.

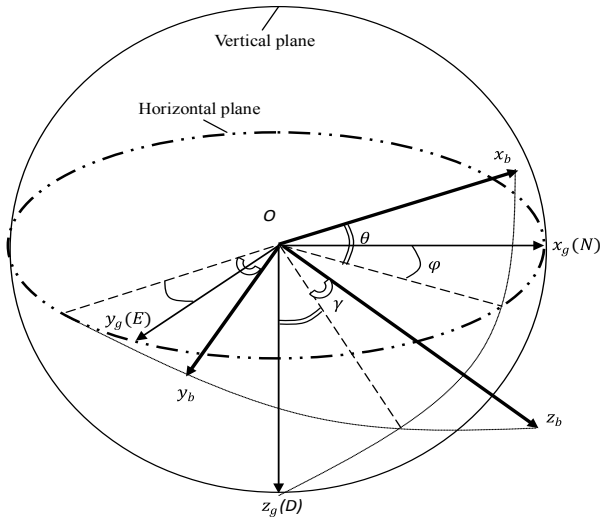

Figure 4: The relationship of the body coordinate system and the ground coordinate system.

which are aligned with true north (N) and true east (E) respectively in this paper. The axis oz_g is perpendicular to the horizontal plane, which points downward (D).

The Euler angular transform matrix determines the orientation of the velocity coordinate system with respect to the body coordinate system,

$$T_{v,b}\left(\alpha_{bw,i},\beta_{bw,i}\right)=\begin{bmatrix}\cos\alpha_{bw,i}\cos\beta_{bw,i} & \sin\beta_{bw,i} & \sin\alpha_{bw,i}\cos\beta_{bw,i}\\ -\cos\alpha_{bw,i}\sin\beta_{bw,i} & \cos\beta_{bw,i} & -\sin\alpha_{bw,i}\sin\beta_{bw,i}\\ -\sin\alpha_{bw,i} & 0 & \cos\alpha_{bw,i}\end{bmatrix}\quad \text{i=1,2} \quad (1)$$

$$\alpha_{bw,i}=\mathrm{tg}^{-1}\left(\frac{V_z+\Omega_i^{*}b_i^{*}\sin\theta_{p,i}}{V_x-\Omega_i^{*}b_i^{*}\cos\theta_{p,i}}\right)\quad \text{i=1,2}$$

$$\beta_{bw,i}=\mathrm{tg}^{-1}\left(\frac{V_y}{\sqrt{\left(V_x-\Omega_i^{*}b_i^{*}\cos\theta_{p,i}\right)^2+\left(V_z+\Omega_i^{*}b_i^{*}\sin\theta_{p,i}\right)^2}}\right),\ i=1,2$$

where $\alpha_{bw,1}$ $\beta_{bw,1}$ are the angle of attack and sideslip angle of body and fore-wing as shown in Figure 3. $\alpha_{bw,2}$ $\beta_{bw,2}$ are the angle of attack and sideslip angle of body and hind-wing as shown in Figure 3. θp_1 is the flapping direction of the fore-wing. θp_2 is the flapping direction of the hind-wing. The detail deriving of the attack angle and the sideslip angle of body and wings is presented in Appendix A.

According to the body coordinate system and the ground coordinate system, the Euler angular transform matrix determines the orientation of the body coordinate system with respect to the ground coordinate system.

$$T_{b,g}(\varphi,\theta,\gamma)=\begin{bmatrix}\cos\varphi\cos\theta & \sin\varphi\cos\theta & -\sin\theta\\ -\sin\varphi\cos\gamma+\cos\varphi\sin\theta\sin\gamma & \cos\varphi\cos\gamma+\sin\varphi\sin\theta\sin\gamma & \cos\theta\sin\gamma\\ \sin\varphi\sin\gamma+\cos\varphi\sin\theta\cos\gamma & -\cos\varphi\sin\gamma+\sin\varphi\sin\theta\cos\gamma & \cos\theta\cos\gamma\end{bmatrix} \quad (2)$$

where ϕ,θ,γ are the heading, pitch and roll angles of dragonfly respectively as shown in Figure 4.

In velocity coordinate system, aerodynamic force can be easily decomposed into lift force, drag force and side force.

$$L_i=\frac{1}{2}\rho\cdot V_i^2\cdot s\cdot C_l\left(\alpha_{w,i}\right)\ \text{I=1,2} \quad (3)$$

$$D_i=\frac{1}{2}\rho\cdot V_i^2\cdot s\cdot C_d\left(\alpha_{w,i}\right)\ \text{i=1,2} \quad (4)$$

$$C_i=\frac{1}{2}\rho\cdot V_i^2\cdot s\cdot C_c\left(\beta_{w,i}\right)\ \text{i = 1,2} \quad (5)$$

$$V_i^2=\left(V_x\sin\theta_{p,i}+V_z\cos\theta_{p,i}\right)^2+V_y^2+\left(-V_x\cos\theta_{p,i}+V_z\sin\theta_{p,i}+\Omega_i\cdot b_i\right)^2\quad \text{i =1,2}$$

where L_1 is the lift force of the fore-wing, D_1 is the drag force of the fore-wing and C_1 is the side force of the fore-wing. V_1 is the local air velocity of the fore-wing. L_2 is the lift force of the hind-wing, D_2 is the drag force of the hind-wing and C_2 is the side force of the hind-wing. V_2 is the local air velocity of the hind-wing. All forces depend on the wing area *s*, the density of air . V_x,V_y,V_z are the velocity of body coordinate system on x-axis, y-axis and z-axis respectively. $C_l(\alpha_{w,1})$, $C_d(\alpha_{w,1})$, $C_c(\beta_{w,1})$ are lift, drag and side force coefficients of the fore-wing, respectively. $C_l(\alpha_{w,2})$, $C_d(\alpha_{w,2})$, $C_c(\beta_{w,2})$ are lift, drag and side force coefficients of the hind-wing, respectively. Ω_1 is the angular velocity of the fore-wing. b_1 is the equivalent span length of the fore-wing. Ω_2 is the angular velocity of the hind-wing. b_2 is the equivalent span length of the hind-wing. we adopt a simplified approximation of these force coefficients [12] as indicated in Eqs. (6), (7) and (8), respectively. The attack angle of the local fore-wing, $\alpha_{w,1}$ the sideslip angle of the local fore-wing, $\beta_{w,1}$ the attack angle of the local hind-wing, ($\alpha_{w,2}$ the sideslip angle of the local hind-wing, $\beta_{w,2}$ are indicated in Eq. (9) and Eq. (10). The detail deriving of the attack angle and the sideslip angle of the wings is presented in Appendix B.

$$C_l\left(\alpha_{w,i}\right)=C_{lmax}\cdot\sin\left(2\cdot\alpha_{w,i}\right)\quad \text{i=1,2} \quad (6)$$

$$C_d\left(\alpha_{w,i}\right)=C_{d0}+C_{dmax}\cdot\sin^2\left(\alpha_{w,i}\right)\quad \text{i=1,2} \quad (7)$$

$$C_c\left(\beta_{w,i}\right)=C_{cmax}\cdot\sin\left(2\cdot\beta_{w,i}\right)\quad \text{i=1,2} \quad (8)$$

$$\alpha_{w,i}=\begin{cases}\mathrm{tg}^{-1}\left(\dfrac{-V_x\cos\theta_{p,i}+V_z\sin\theta_{p,i}+\Omega_i\cdot b_i}{V_x\sin\theta_{p,i}+V_z\cos\theta_{p,i}}\right)-\alpha_{\text{off1}} & \text{downstroke}\\ \mathrm{tg}^{-1}\left(\dfrac{-V_x\cos\theta_{p,i}+V_z\sin\theta_{p,i}+\Omega_i\cdot b_i}{V_x\sin\theta_{p,i}+V_z\cos\theta_{p,i}}\right)+\alpha_{\text{off2}} & \text{upstroke}\end{cases}\quad \text{i=1,2} \quad (9)$$

$$\beta_{w,i}=\mathrm{tg}^{-1}\left(\frac{V_y}{\sqrt{\left(V_x\sin\theta_{p,i}+V_z\cos\theta_{p,i}\right)^2+\left(-V_x\cos\theta_{p,i}+V_z\sin\theta_{p,i}+\Omega_i\cdot b_i\right)^2}}\right)\quad \text{i=1,2} \quad (10)$$

The parameters α_{off1} and α_{off2} in Eq. (9) are average torsional angles

during downstroke and upstroke because of the characteristics of wing's deformation. We adopt the maximum lift coefficient C_{lmax}=2 maximum drag coefficient C_{dmax}=2 the maximum side force coefficient C_{max}=0.5 and the zero drag coefficient C_{d0}=0.05 in simulations [12].

Remark 2: In our work, the aerodynamic force is a function of the local air velocity of the wing and local attack angle of the wing. In contrast, in some existing works [7,11,12], the aerodynamic force is a continuous function of the freedom air velocity. The problem associated with the existing aerodynamic force model is the loss of ability in hovering. Note that the freedom air velocity is zero when the dragonfly is hovering. Thus, according to this mathematical model, the aerodynamic force is zero during hovering, and the dragonfly would drop. To remove this unrealistic situation, we incorporate the local air velocity of the fore-wing and hind-wing, V_1 and V_2 into the model of aerodynamic force.

Mathematical model

According to the transform of ground coordinate system and body coordinate system in Eq. (2), we obtain the kinematic equations of dragonfly's centroid and the kinematic equations of dragonfly's rotation around its centroid.

$$\begin{bmatrix}\dot{x}_g\\ \dot{y}_g\\ \dot{z}_g\end{bmatrix}=\begin{bmatrix}\cos\varphi\cos\theta & -\sin\varphi\cos\gamma+\cos\varphi\sin\theta\sin\gamma & \sin\varphi\sin\gamma+\cos\varphi\sin\theta\cos\gamma\\ \sin\varphi\cos\theta & \cos\varphi\cos\gamma+\sin\varphi\sin\theta\sin\gamma & -\cos\varphi\sin\gamma+\sin\varphi\sin\theta\cos\gamma\\ -\sin\theta & \cos\theta\sin\gamma & \cos\theta\cos\gamma\end{bmatrix}\cdot V \quad (11)$$

$$\begin{bmatrix}\dot{\varphi}\\ \dot{\theta}\\ \dot{\gamma}\end{bmatrix}=\begin{bmatrix}0 & \dfrac{\sin\gamma}{\cos\theta} & \dfrac{\cos\gamma}{\cos\theta}\\ 0 & \cos\gamma & -\sin\gamma\\ 1 & \sin\gamma\cdot\mathrm{tg}\theta & \cos\gamma\cdot\mathrm{tg}\theta\end{bmatrix}\cdot W \quad (12)$$

where x_g, y_g, z_g are the position of dragonfly in the ground coordinate system. $V=[V_x\ V_y\ V_z]'$ is the velocity of dragonfly in the body coordinate system. ψ,θ,γ are the heading, pitch and roll angles of dragonfly, respectively. $W=[w_x w_y w_z]'$ is the angular velocity of dragonfly in the body coordinate system.

For simplicity, we adopt the following assumptions to model the dragonfly.

Assumption1: The aerodynamic forces are the average of a cyclic aerodynamic force during the flapping stroke.

Assumption 2: Each pair of wings has the same sweeping direction and flapping frequency.

Under above assumptions, the dynamic equation of the motion is obtained according to the Euler angular transform matrices in Eq. (1), Eq. (2), and Newton's second law.

$$m\left(\dot{V}+W\times V\right)=F_1+F_2+T_{b,g}(\varphi,\theta,\gamma)\begin{bmatrix}0\\0\\mg\end{bmatrix} \quad (13)$$

$$F_1=T'_{v,b}\left(\alpha_{bw,1},\beta_{bw,1}\right)\begin{bmatrix}-D_1\\-C_1\\-L_1\end{bmatrix},\ F_2=T'_{v,b}\left(\alpha_{bw,2},\beta_{bw,2}\right)\begin{bmatrix}-D_2\\-C_2\\-L_2\end{bmatrix}$$

where D_i, C_i, L_i (i=1,2) are given in Eq. (3), Eq. (4), Eq. (5), and $\alpha_{bw,i}$, $\beta_{bw,i}$ (i=1,2) are given in Eq. (1). F_1 is the aerodynamic force of the fore-wing in the body coordinate system. F_2 is the aerodynamic force of the hind-wing in the body coordinate system.

The dynamic equations of dragonfly's rotating around its centroid are obtained in the body coordinate system by using the Euler angular transform matrices in Eq. (1), Eq. (2) and the moment of momentum theorem.

$$\begin{bmatrix}I_x & -I_{xy} & -I_{zx}\\ -I_{xy} & I_y & -I_{yz}\\ -I_{zx} & -I_{yz} & I_z\end{bmatrix}\cdot\dot{W}+W\times\left\{\begin{bmatrix}I_x & -I_{xy} & -I_{zx}\\ -I_{xy} & I_y & -I_{yz}\\ -I_{zx} & -I_{yz} & I_z\end{bmatrix}\cdot W\right\}=M \quad (14)$$

where $I_x I_y I_z I_{xy} I_{yz} I_{zx}$ are the relative moment of inertia of the dragonfly. $M=[M_x M_y M_z]'$ is the moment in the body coordinate system as shown in Figure 1. These moments are described as follows according to the moment of momentum theorem.

$$M=\begin{bmatrix}x_{gc}-x_{g1}\\ y_{gc}-y_{g1}\\ z_{gc}-z_{g1}\end{bmatrix}\times F_1+\begin{bmatrix}x_{gc}-x_{g2}\\ y_{gc}-y_{g2}\\ z_{gc}-z_{g2}\end{bmatrix}\times F_2+\begin{bmatrix}x_{gc}-x_{tail}\\ y_{gc}-y_{tail}\\ z_{gc}-z_{tail}\end{bmatrix}\times\left\{T_{b,g}(\varphi,\theta,\gamma)\begin{bmatrix}0\\0\\m_{tail}g\end{bmatrix}\right\}+\begin{bmatrix}x_{gc}-x_{nose}\\ y_{gc}-y_{nose}\\ z_{gc}-z_{nose}\end{bmatrix}\times\left\{T_{b,g}(\varphi,\theta,\gamma)\begin{bmatrix}0\\0\\m_{nose}g\end{bmatrix}\right\}$$

In above equations of aerodynamic moment, x_{g1}、y_{g1}、z_{g1} are positions of the fore-wing aerodynamic pressure. $x_{g2}y_{g2}z_{g2}$ are positions of the hind-wing aerodynamic pressure. $x_{gc}y_{gc}z_{gc}$ are positions of the central of dragonfly's gravity. $x_{tail}y_{tail}z_{tail}$ are positions of the central of dragonfly tail's gravity. $x_{nose}y_{nose}z_{nose}$ are positions of the central of dragonfly head's gravity. Then the positions of the central of dragonfly tail and head gravity, which are shown in Figure 5, are described as follows.

$$x_{tail}=x_{offset}+0.5\,r_{tail}\cos\theta_{tail}\cos\varphi_{tail}$$

$$y_{tail}=-0.5\,r_{tail}\cos\theta_{tail}\sin\varphi_{tail}$$

$$z_{tail}=-0.5\,r_{tail}\sin\theta_{tail}$$

$$x_{nose}=x_{offnose}-0.5\,r_{nose}\cos\theta_{nose}\cos\varphi_{nose}$$

$$y_{nose}=0.5\,r_{nose}\cos\theta_{nose}\sin\varphi_{nose}$$

$$z_{nose}=-0.5\,r_{nose}\sin\theta_{nose}$$

x_{offset} is the offset between the tail and the centre of body gravity. r_{tail} is the length of the tail. φ_{tail} is the yaw angle of the dragonfly's tail. θ_{tail} is the pitch angle of the dragonfly's tail. $x_{offnose}$ is the offset between the head and the centre of body gravity. r_{nose} is the length of the head. φ_{nose} is the yaw angle of the dragonfly's head. θ_{nose} is the pitch angle of the dragonfly's head.

Controller Design for the Dragonfly-like FWMAV

From Eqs. (11)~(14), the mathematical model of dragonfly is highly

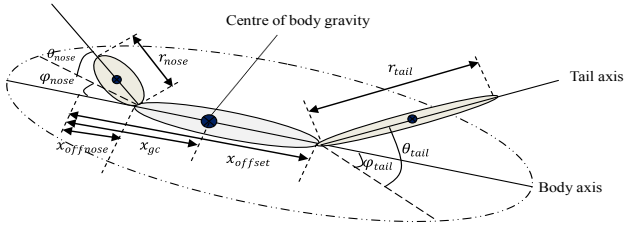

Figure 5: Sketch map of the centre of tail, head and body gravity.

nonlinear. Nonlinear control is one of the biggest challenges in control theory and applications. To control the dragonfly-like FWMAV, the target variables are the flapping angular velocity, flapping direction of fore-wings and hind-wings, the yaw and pitch angle of tail, and the yaw angle of the dragonfly's head accordingly to the angle error and velocity error.

Modeling of control system

According to the above aerodynamic force and mathematical model of dragonfly, the state-space equations are

$$\dot{x}=f(x)+h(x,u) \tag{15}$$

Where $\boldsymbol{x}=\left[x_g \quad y_g \quad z_g \quad \varphi \quad \theta \quad \gamma \quad V_x \quad V_y \quad V_z \quad w_x \quad w_y \quad w_z\right]'$ is the state vector, $u=[\Omega_1\ \theta_{(p,1)}\ \Omega_2\ \theta_{(p,2)}\ \psi_{tail}\ \theta_{tail}\ \psi_{nose}]'$ is the control vector. We choose $I_{xy} = 0$ and $I_{yz} = 0$ because the body of dragonfly is symmetric. f(x) and h (x,u) are described in Appendix C in detail.

This is a system of first order non-linear differential equations, where the right hand side depends on the control vector *u*.

Remark 3: This remark is the reason that the control vector is $u=[\Omega_1\ \theta_{(p,1)}\ \Omega_2\ \theta_{(p,2)}\ \psi_{tail}\ \theta_{tail}\ \psi_{nose}]'$.

Firstly, Michael H. Dickinson et al mention the wings' movement of an insect [14]. They suggest that the wing stroke of an insect is typically divided into four kinematic portions: two translational phases (upstroke and down stroke), when the wings sweep through the air with a high angle of attack, and two rotational phases (pronation and supination), when the wings rapidly rotate and reverse direction. It also point out that two degrees of freedom in each wing of most insects are used to achieve flight in the nature: flapping and feathering [15,16]. Flapping is rotation of a wing about longitudinal axis of the body. We consider it as the flapping angular velocity. Feathering is angular movement about the wing longitudinal axis. We consider it as the flapping direction of the wings. Secondly, Robert M Olberg mentions the head movement of dragonfly during preying the target [17]. He suggests that the target distance estimation is obtained by using motion parallax information from a head bob during preying, because the head rotates to stabilize the prey image. We consider it as the yaw angle of the dragonfly's head. Lastly, by our observation and common knowledge, we can also find that the yaw and pitch angle of tail are adjustable or deformable during the dragonfly flight in the nature. So we consider them all to be control input.

Controller design

The design method of nonlinear dynamic inversion is applied to our system due to the character of the high nonlinearity. Define the state error and its derivative

$$\boldsymbol{e}=\boldsymbol{x}-\boldsymbol{x}_{ref}$$

$$\dot{\boldsymbol{e}}=\dot{\boldsymbol{x}}-\dot{\boldsymbol{x}}_{ref}z \tag{16}$$

where x_{ref} is the desired state vector.

Substituting Eq. (15) into Eq. (16) yields

$$\dot{\boldsymbol{e}}=\dot{\boldsymbol{x}}-\dot{\boldsymbol{x}}_{ref}=\boldsymbol{f}(\boldsymbol{x})+\boldsymbol{h}(\boldsymbol{x},\boldsymbol{u})-\dot{\boldsymbol{x}}_{ref}\cdot$$

In order to assure an exponential error convergence, the control input should be design to meet the following relationship

$$\boldsymbol{f}(\boldsymbol{x})+\boldsymbol{h}(\boldsymbol{x},\boldsymbol{u})-\dot{\boldsymbol{x}}_{ref}=-\lambda\cdot\boldsymbol{e} \tag{17}$$

where λ is a positive constant.

The objective is now to find control *u* that can manipulate the dragonfly's wings, tail and head. Here we employ a Newton-Raphson solver to obtain control input *u* in Eq. (17). The iteration formulation of control input is described as follow.

$$\boldsymbol{u}_{k+1}=\boldsymbol{u}_k-\left(J_k'\cdot J_k\right)^{-1}\cdot J_k'\cdot\left[\boldsymbol{f}(\boldsymbol{x}_k)+\boldsymbol{h}(\boldsymbol{x}_k,\boldsymbol{u}_k)-\dot{\boldsymbol{x}}_{ref}+\lambda\cdot\boldsymbol{e}_k\right] \tag{18}$$

$$\boldsymbol{e}_k=\boldsymbol{x}_k-\boldsymbol{x}_{ref}$$

$$J_k=\left.\frac{\partial\boldsymbol{h}(\boldsymbol{x},\boldsymbol{u})}{\partial\boldsymbol{u}}\right|_{\boldsymbol{x}=\boldsymbol{x}_k,\boldsymbol{u}=\boldsymbol{u}_k}$$

where j_k is the Jacobian matrix. When the precision of control input is met, $\left|\boldsymbol{u}_{k+1}-\boldsymbol{u}_k\right|<\varepsilon$ the control input is obtained.

By substituting Eqs. (11)~(13) and (14) into Eq. (18), we obtain the Jacobian matrix. However, the Jacobian matrix J_k is singular because many elements h(x,u) are zeros. Thus it is not possible to obtain the control vector *u* by Eq. (18). To capture the insight into the control system design, we transform the Eq. (15) into a control companion form since the state vector is reduced by removing the position and the y-axis velocity of dragonfly.

$$\dot{\boldsymbol{x}}_1=\boldsymbol{f}_1(\boldsymbol{x}_1,\boldsymbol{x}_2) \tag{19}$$

$$\begin{bmatrix}\dot{\boldsymbol{x}}_2\\ \dot{\boldsymbol{x}}_3\end{bmatrix}=\boldsymbol{f}_2(\boldsymbol{x}_1,\boldsymbol{x}_2,\boldsymbol{x}_3)+\boldsymbol{h}_2(\boldsymbol{x}_1,\boldsymbol{x}_2,\boldsymbol{x}_3,\boldsymbol{u}) \tag{20}$$

where $\boldsymbol{x}_1=\left[\varphi \quad \theta \quad \gamma\right]'$ is the first set of the states; $\left[\boldsymbol{x}_2' \quad \boldsymbol{x}_3'\right]'=\left[w_x \quad w_y \quad w_z \quad V_x \quad V_z\right]'$ is the second set of the states; $\boldsymbol{x}_2=\left[w_x \quad w_y \quad w_z\right]'$ and $x_3=[V_x\ V_z)]'$. The right function, $\boldsymbol{f}_1(\boldsymbol{x}_1,\boldsymbol{x}_2)$, of Eq. (19) is consist of the 4-th, 5-th and 6-th elements of the right function, f(x) of Eq. (15) respectively. The right function, $\boldsymbol{f}_2(\boldsymbol{x}_1,\boldsymbol{x}_2,\boldsymbol{x}_3)$, of Eq. (20) is consist of the 10-th, 11-th, 12-th, 7-th and 9-th elements of the right function f(x) of Eq. (15) respectively. The right function, $\boldsymbol{h}_2(\boldsymbol{x}_1,\boldsymbol{x}_2,\boldsymbol{x}_3,\boldsymbol{u})$, of Eq. (20) is consist of the 10-th, 11-th, 12-th, 7-th and 9-th elements of the right function, h(x,u) of Eq. (15) respectively.

Note that x_2 in Eq. (19) is a virtual control input the x_1 sub-dynamics. Thus we adopt a dual loop iteration, where outer loop solves for the actual control input $\boldsymbol{u}$, and inner loop solves for the virtual control input x_2. Based on Eq. (19) and Eq. (20), we derive the outer and inner loop control vectors respectively as

$$\boldsymbol{u}_{k+1}=\boldsymbol{u}_k-\left(J_{2,k}'\cdot J_{2,k}\right)^{-1}\cdot J_{2,k}'\cdot\left[\boldsymbol{f}_2(\boldsymbol{x}_{1,k},\boldsymbol{x}_{2,k},\boldsymbol{x}_{3,k})+\boldsymbol{h}_2(\boldsymbol{x}_{1,k},\boldsymbol{x}_{2,k},\boldsymbol{x}_{3,k},\boldsymbol{u}_k)-\begin{bmatrix}\dot{\boldsymbol{x}}_{2,ref}\\ \dot{\boldsymbol{x}}_{3ref}\end{bmatrix}+\lambda_2\cdot\boldsymbol{e}_{2,k}\right]$$

$$\boldsymbol{x}_{2,k+1}=\boldsymbol{x}_{2,k}-\left(J_{1,k}'\cdot J_{1,k}\right)^{-1}\cdot J_{1,k}'\cdot\left[\boldsymbol{f}_1(\boldsymbol{x}_{1,k},\boldsymbol{x}_{2,k})-\dot{\boldsymbol{x}}_{1,ref}+\lambda_1\cdot\boldsymbol{e}_{1,k}\right]$$

$$J_{1,k}=\left.\frac{\partial\boldsymbol{f}_1(\boldsymbol{x}_1,\boldsymbol{x}_2)}{\partial\boldsymbol{x}_2}\right|_{\boldsymbol{x}_1=\boldsymbol{x}_{1,k},\boldsymbol{x}_2=\boldsymbol{x}_{2,k}}$$

$$J_{2,k}=\left.\frac{\partial\boldsymbol{h}_2(\boldsymbol{x}_1,\boldsymbol{x}_2,\boldsymbol{x}_3,\boldsymbol{u})}{\partial\boldsymbol{u}}\right|_{\boldsymbol{x}_1=\boldsymbol{x}_{1,k},\boldsymbol{x}_2=\boldsymbol{x}_{2,k},\boldsymbol{x}_3=\boldsymbol{x}_{3,k},\boldsymbol{u}=\boldsymbol{u}_k}$$

$$\boldsymbol{x}_{1,ref}=\left[\varphi_{ref} \quad \theta_{ref} \quad \gamma_{ref}\right]'$$

$$\dot{\boldsymbol{x}}_{1,ref}=\left[\dot{\varphi}_{ref} \quad \dot{\theta}_{ref} \quad \dot{\gamma}_{ref}\right]'$$

$$\boldsymbol{x}_{2,ref}=\begin{bmatrix}-\sin\theta & 0 & 1\\ \cos\theta\cdot\sin\gamma & \cos\gamma & 0\\ \cos\theta\cdot\cos\gamma & -\sin\gamma & 0\end{bmatrix}\cdot\begin{bmatrix}\dot{\varphi}_{ref}\\ \dot{\theta}_{ref}\\ \dot{\gamma}_{ref}\end{bmatrix}$$

$$\dot{\boldsymbol{x}}_{2,ref} = \begin{bmatrix} -\cos\theta & 0 & 0 \\ -\sin\theta\cdot\sin\gamma & \cos\theta\cdot\cos\gamma & -\sin\gamma \\ -\sin\theta\cdot\cos\gamma & -\cos\theta\cdot\sin\gamma & -\cos\gamma \end{bmatrix} \cdot \begin{bmatrix} \dot{\varphi}_{ref}\cdot\dot{\theta}_{ref} \\ \dot{\varphi}_{ref}\cdot\dot{\gamma}_{ref} \\ \dot{\theta}_{ref}\cdot\dot{\gamma}_{ref} \end{bmatrix}$$

$$\boldsymbol{x}_{3,ref} = \begin{bmatrix} V_{x,ref} & V_{z,ref} \end{bmatrix}'$$

$$\dot{\boldsymbol{x}}_{3,ref} = \begin{bmatrix} \dot{V}_{x,ref} & \dot{V}_{z,ref} \end{bmatrix}'$$

Where $J_{1,k}$ and $J_{2,k}$ are the corresponding Jacobian matrices, λ_1 and λ_2 are positive constants, $\boldsymbol{e}_{1,k} = \boldsymbol{x}_{1,k} - \boldsymbol{x}_{1,ref}$ and $\boldsymbol{e}_{2,k} = \begin{bmatrix} \boldsymbol{x}'_{2,k} & \boldsymbol{x}'_{3,k} \end{bmatrix}' - \begin{bmatrix} \boldsymbol{x}'_{2,ref} & \boldsymbol{x}'_{3,ref} \end{bmatrix}'$ are the state error vectors. When the precision of control input is met, $|\boldsymbol{u}_{k+1} - \boldsymbol{u}_k| < \varepsilon$, the control input $\boldsymbol{u} = \frac{\boldsymbol{u}_{k+1} + \boldsymbol{u}_k}{2}$ is obtained.

Numerical Simulation Examples

In order to verify the validity of the dynamic model and the control algorithm, simulation study is performed in this section. There are three scenarios in the section. In the first scenario FWMAV is under open-loop control. The reference is a set-point in the second scenario and a time-varying trajectory in the third scenario. The dynamic model parameters are given as x_{offset} = 0.12 m, r_{tail} = 0.65 m, $x_{offnose}$= 0.06 m, r_{nose}= 0.08 m, m = 0.20843 kg, m_{tail}= 0.01 kg, m_{nose}= 0.02 kg, s = 0.15 m^2, x_{g1}=0.02 m, y_{g1}=0.0 m, z_{g1}=0.005 m, x_{g2}=0.09 m, y_{g2}=0.0 m, z_{g2}=0.005 m, x_{gc}=0.03556 m, y_{gc}=0.0 m, z_{gc}= 0.005 m, I_x = 0.0005 kg·m^2, I_y= 0.0068 kg·m^2, I_z = 0.0059 kg·m^2, I_{zx}= 0.000012 kg·m^2, b = 0.32 m, λ_1=7.5, λ_2= 2.5. The precision of control input is ε = 0.0001.

Open-loop control

To evaluate the validity of the dragonfly-like FWMAV model, open-loop control with constant control inputs is applied, in which three different pitch angles are given. In the first test the pitch is 1.0 rad, namely FWMAV is nose-up. In the second test the pitch is -0.5 rad, namely FWMAV is nose-down. In the third test the pitch is 0.0 rad, namely FWMAV is horizontal. The simulation results are depicted in Figures 6a-6c. The control input vector is u(t) = [11.2951 rad/s, 1.6049 rad, 13.7869 rad/s, 1.6120 rad, 0.0 rad, 0.0 rad, 0.0 rad]'. The initial states vector are x_1 (0) = [0.0 rad, 1.0 rad, 0.0 rad]', x_2 (0) = [0.0 rad/s, 0.0 rad/s, 0.0 rad/s]' and x_3 (0) = [6.0 m/s, 0.0 m/s]' in Figure 6a. The initial states vector are x_1 (0) = [0.0 rad, -0.5 rad, 0.0 rad]', x_2 (0) = [0.0 rad/s, 0.0 rad/s, 0.0 rad/s]' and x_3 (0) = [6.0 m/s, 0.0 m/s]' in Figure 6b. The initial states vector are x_1 (0) = [0.0 rad, 0.0 rad, 0.0 rad]', x_2 (0) = [0.0 rad/s, 0.0 rad/s, 0.0 rad/s]' and x_3 (0) = [0.0 m/s, 0.0 m/s]' in Figure 6c.

It can be observed that there exists steady state or a stable phase, in which the velocities and pitch angle converge to constant values. The values of steady state velocities and pitch angle are determined by the control input signals.

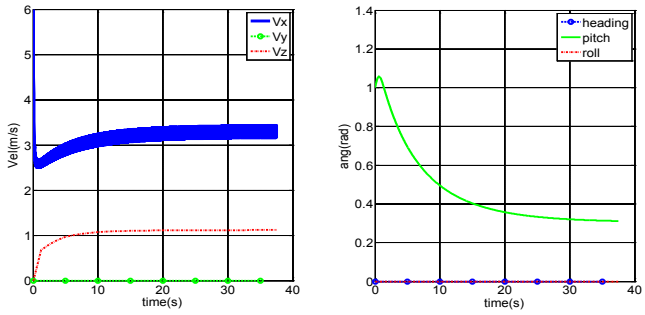

Figure 6a: Velocity and angular curves of FWMAV, x_1 (0)=[0.0 rad 1.0 rad 0.0 rad]', x_2 (0)=[0.0 rad/s 0.0 rad/s 0.0 rad/s]', x_3 (0)=[6.0 m/s 0.0 m/s]'.

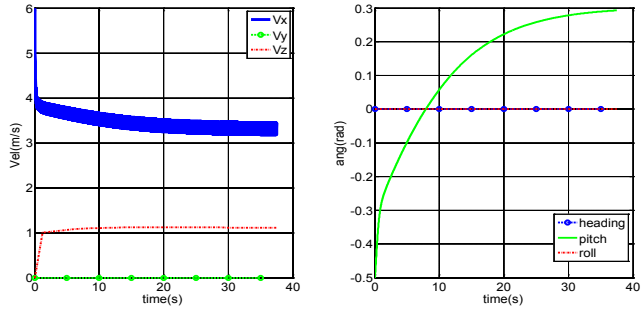

Figure 6b: Velocity and angular curves of FWMAV, x_1 (0)=[0.0 rad -0.5 rad 0.0 rad]', x_2 (0)=[0.0 rad/s 0.0 rad/s 0.0 rad/s]', x_3 (0)=[6.0 m/s 0.0 m/s]'.

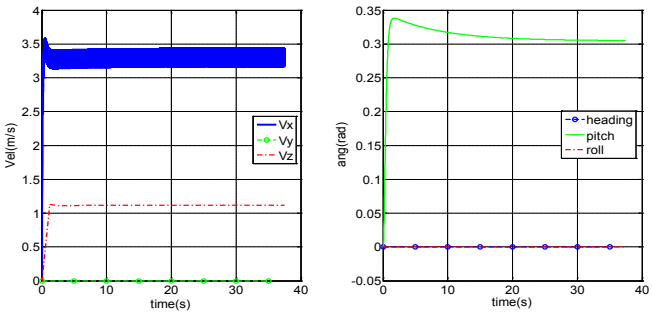

Figure 6c: Velocity and angular curves of FWMAV, x_1 (0)=[0.0 rad 0.0 rad 0.0 rad]', x_2 (0)=[0.0 rad/s 0.0 rad/s 0.0rad/s]', x_3 (0)=[0.0 m/s 0.0 m/s]'.

Next we observe transient phase behavior. First, it can be easily found that the pitch angle of FWMAV rises during the initial stage, then the pitch angle drops in Figures 6a and 6c, while the pitch angle keeps increasing in Figure 6b. The reason for pitch up during the initial stage is because the moment of the hind-wings is less than the summed moment of the fore-wings and the tail. After the initial phase, pitch angles in Figures 6a and 6c, which exceed 0.3 rad, will drop or converge to the stable phase angle that is around 0.3 rad.

It is noted that V_z namely the z-axis velocity in the body coordinate system, rises more rapidly in Figures 6b and 6c, because in case (Figure 6a) FWMAV is nose-up with the largest absolute pitch angle, hence the gravity incurs a smallest push force along the direction of V_z as the gravity projects onto V_z with a factor of the cosine of the pitch angle. Next by observation, the x-axis velocity V_x in the body coordinate system drops more rapidly in Figure 6a than that in Figure 6b. This is because the absolute attack angle in Figure 6a is larger than that in Figure 6b, hence incurs a large air resistance along the longitudinal direction. In the case of Figure 6c, the initial V_x is zero, and increases quickly because the wings' flapping generates a thrust along the direction of V_x.

The tail and head of our dragonfly-like FWMAV are not deflected according the control input in this scenario. The side force and the moments M_x, M_z are zero. It results in that the V_y is zero due to zero side force, the heading angle is zero due to zero moment M_z and zero initial heading angle, the roll angle is zero due to zero moment M_x and zero initial roll angle.

The above discussions illustrate the consistency between the model-based simulation results and motion behaviors of FWMAV derived from physical principles, thus verify the validity of the FWMAV model derived in this work.

Set-point control

In this scenario the reference vector is constant. In this scenario we evaluate the basic capability of the dragonfly to quickly respond to the given reference with the proposed control algorithm. The simulation results are depicted in Figures 7a-7c. The initial states vector are x_1 (0) = [0.0 rad, 0.01 rad, 0.0 rad]', x_2 (0) = [0.0 rad/s, 0.0 rad/s, 0.0 rad/s]' and x_3 (0) = [0.01 m/s, -0.01 m/s]' u(t) = [11.2951 rad/s, 1.6049 rad, 13.7869 rad/s, 1.6120 rad, 0.0 rad, 0.0 rad, 0.0 rad]' is the initial control input vector. The reference pitch angle is θ_{ref} = 1.3 rad, and the reference roll angle is γ_{ref} = 0.3 rad. The reference velocity is $V_{x,ref}$ = 2.0 m/s and $V_{z,ref}$ = 0.0 m/s.

Trajectory tracking

To evaluate the tracking performance of the proposed control algorithm the time-varying reference vector is considered in this scenario. Figure 8 shows the actual angle of dragonfly and reference angle trajectory. In this scenario initial states of the flapping wings MAV are the same as the second scenario. The desired pitch and roll angle are θ_{ref}=0.8+0.4 sin(0.1t) , γ_{ref}=0.5+0.2 sin(0.1t)

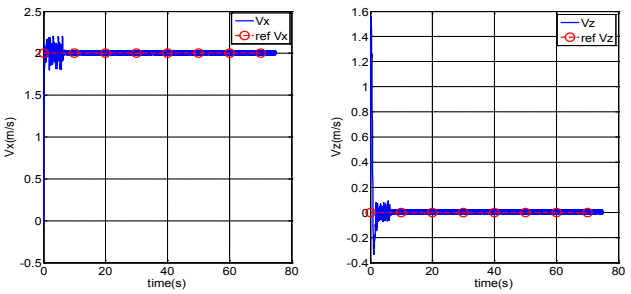

Figure 7a: Velocity response curves of FWMAV, $V_{x,ref}$=2.0 m/s and $V_{z,ref}$=0.0 m/s.

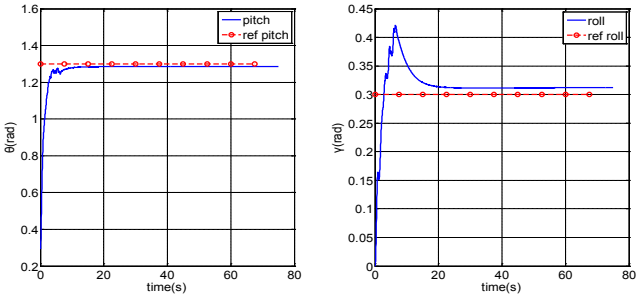

Figure 7b: Angular response curves of FWMAV, θ_{ref}=1.3 rad, γ_{ref}=0.3 rad.

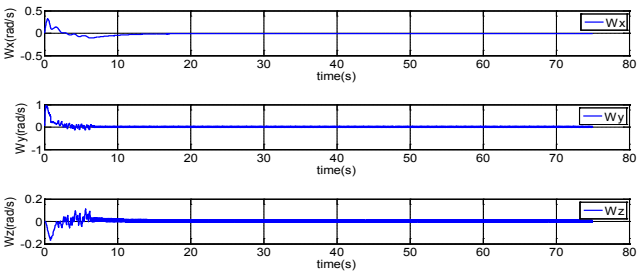

Figure 7c: Response curves of angular velocity of FWMAV.

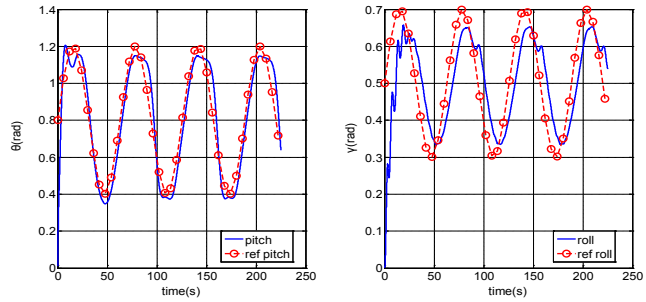

Figure 8: Response curves of angle of FWMAV and reference angle, θ_{ref}=0.8+0.4 sin (0.1t), γ_{ref}=0.5+0.2 sin (0.1t).

We can find that the states of our flapping wings MAV rapidly converge to the references respectively from Figures 7a and 7b with the constant references, and Figure 8 with the time-varying reference values. It is indicated that the proposed controller is feasible and valid. Figure 7b shows that the angles of dragonfly-like FWMAV are stable at the desired values. From Figures 7a and 7c, the velocity and angular velocity fluctuate slightly around their desired values. The reason for fluctuation is due to the aerodynamic forces and moments of the FWMAV that fluctuate during the upstroke and the down stroke of a flapping cycle, as well as the changing aerodynamic direction and value of wings.

Conclusion

This paper focuses on the nonlinear modeling and control of a dragonfly-like flapping wing MAV. Due to the nonlinear character of the model, the control design method incorporating nonlinear dynamic inversion and Newton-Raphson solution is employed. Numerical results show the effectiveness and convergence performance of dragonfly-like FWMAV flight controller.

In the future we expect to explore the coupling effect of aerodynamic force and moment between the fore-wing and hind-wing in order to improve the aerodynamic model of the dragonfly-like FWMAV. In addition, we will address the issue on how to design the controller of dragonfly-like FWMAV in which two pairs of wings can be manipulated independently [17-19].

References

1. Groen M, Bruggeman B, Remes B, Ruijsink R, Oudheusden BV, et al. (2010) Improving Flight Performance of the Flapping Wing MAV DelFly II. International Micro Air Vehicle conference and competitions.
2. Schenato L, Wu WC, Sastry SS (2004) Attitude Control for a Micromechanical Flying Insect via Sensor Output Feedback. IEEE Transactions on Robotics and Automation 20: 93-106.
3. Keennon M, Klingebiel K, Won H, Andriukov A (2012) Development of the Nano Hummingbird: a Tailless Flapping Wing Micro Air Vehicle. The 50th AIAA Aerospace Sciences Meeting, Nashville, Tennessee.
4. Techjet's Dragonfly.
5. Festo's Bionic Opter.
6. Jang JS, Tomlin CJ (2003) Longitudinal Stability Augmentation System Design for the DragonFly UAV Using a Single GPS Receiver. AIAA Guidance Navigation and Control Conference, Texas.

7. Couceiro MS, Ferreira MS, Tenreiro JA (2010) Modeling and Control of a Dragonfly-Like Robot. Journal of Control Science and Engineering 2010: 1-11.
8. Nguyen QV, Chan W, Debiasi M (2014) Design Fabrication and Performance Test of a Hovering-Based Flapping-Wing Micro Air Vehicle Capable of Sustained and Controlled Flight. IMAV 2014: 18-25.
9. Leong CW, Viet NQ, Debiasi M (2014) Pitch and Yaw Control of Tailless Flapping Wing MAVs by Implementing Wing Root Angle Deflection. IMAV.
10. Sun JY, Pan CX, Tong J, Zhang J (2010) Coupled Model Analysis of the Structure and Nano-mechanical Properties of Dragonfly Wings. IET Nanobiotechnology 4: 10-18.
11. Okamoto M, Yasuda K, Azuma A (1996) Aerodynamic Characteristics of the Wings and Body of a Dragonfly. The journal of experimental biology 199: 281-294.
12. Couceiro MS, Ferreira NMF, Machado JAT (2012) Hybrid Adaptive Control of a Dragonfly Model. Commun Nonlinear Sci Numer Simulat 17: 893-903.
13. Chirarattananon P, Kevin Y M, Wood RJ (2014) Adaptive Control of a Millimeter-scale Flapping-wing Robot. Bioinspiration and Biomimetics 9: 1-16.
14. Dickinson MH, Lehmann FO, Sane SP (1999) Wing Rotation and the Aerodynamic Basis of Insect Flight. Science 284: 1954-1960.
15. Khan ZA, Agrawal SK (2005) Modeling and Simulation of Flapping Wing Micro Air Vehicles. International Design Engineering Technical Conferences & Computers and Information in Engineering Conference, Long Beach, California, USA.
16. Duan H, Qingwei Li (2009) Dynamic Model and Attitude Control of Flapping Wing Micro Aerial Vehicle. IEEE International Conference on Robotics and Biomimetics, Guilin, China.
17. Olberg RM (2012) Visual Control of Prey-capture Flight in Dragonflies. Neurobiology 22: 267-271.
18. Naka H, Hashimoto H (2015) Effects of Deformation and Vibration Characteristics of Wings on Flapping Flight. J-Stage Advance Publication 9: 1-12.
19. Zeyghami S, Dong H (2015) Study of Turning Takeoff Maneuver in Free-flying Dragonflies Effect of Dynamic Coupling. Fluid Dynamics 24: 1-19.

This article was originally published in a special issue, entitled: "Robotics in Surgery", Edited by Buchs Nicolas, University Hospitals of Geneva, Switzerland